iScience

CellPress
OPEN ACCESS

Article

Using structure-function relationships to understand the mechanism of phenazine-mediated extracellular electron transfer in *Escherichia coli*

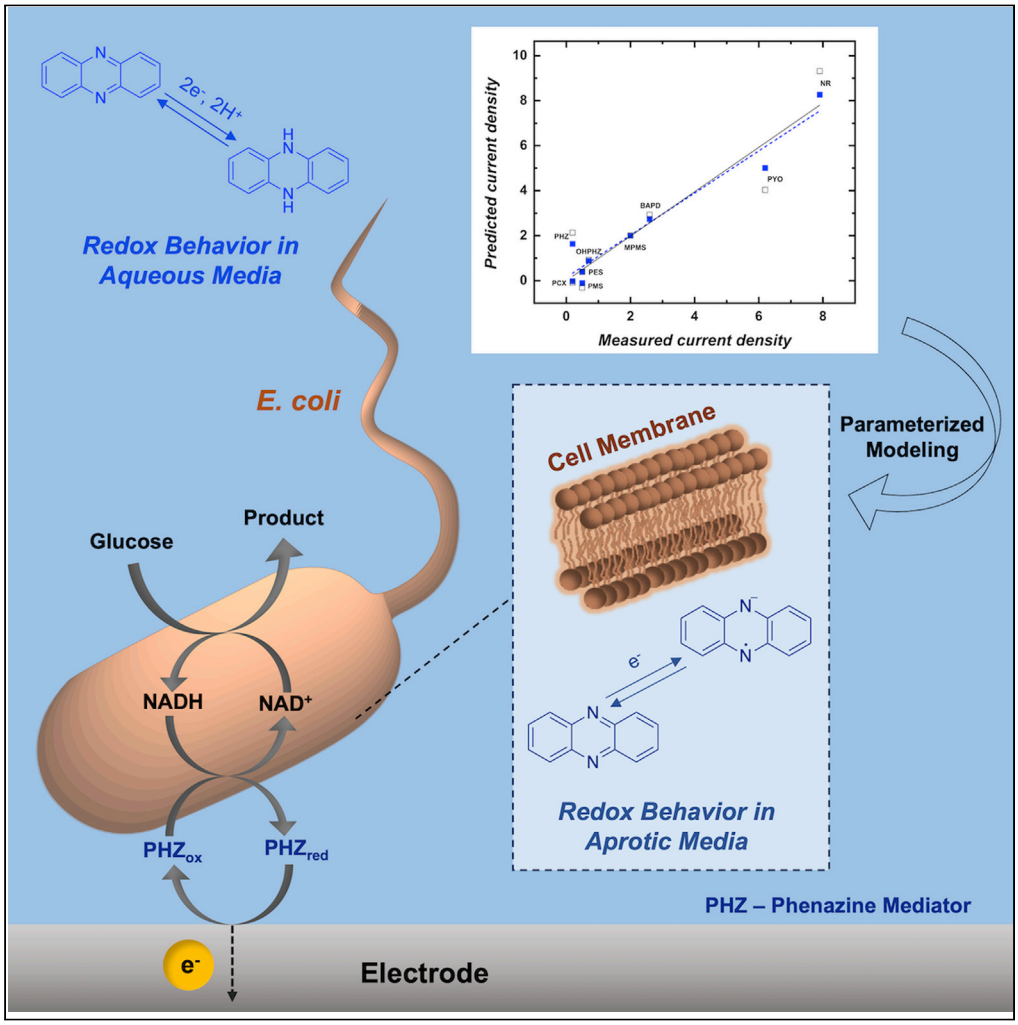

Zayn Rhodes, Olja Simoska, Ashwini Dantanarayana, Keith J. Stevenson, Shelley D. Minteer

olja.simoska@utah.edu (O.S.)
minteer@chem.utah.edu (S.D.M.)

Highlights

Coupling experimental data on phenazine-mediated EET in *E. coli* with DFT computations

Computational data suggest that electron transfer occurs in lipophilic cell membrane

Developed predictive mediated current density model for phenazine mediators

The model can be used in future design of mediated microbial electrochemical systems

Rhodes et al., iScience *24*, 103033
September 24, 2021
https://doi.org/10.1016/j.isci.2021.103033

iScience

CellPress
OPEN ACCESS

Article

Using structure-function relationships to understand the mechanism of phenazine-mediated extracellular electron transfer in *Escherichia coli*

Zayn Rhodes,[1,3] Olja Simoska,[1,3,*] Ashwini Dantanarayana,[1] Keith J. Stevenson,[2] and Shelley D. Minteer[1,4,*]

SUMMARY

Phenazines are redox-active nitrogen-containing heterocyclic compounds that can be produced by either bacteria or synthetic approaches. As an electron shuttles (mediators), phenazines are involved in several biological processes facilitating extracellular electron transfer (EET). Therefore, it is of great importance to understand the structural and electronic properties of phenazines that promote EET in microbial electrochemical systems. Our previous study experimentally investigated a phenazine-based library as an exogenous mediator system to facilitate EET in *Escherichia coli*. Herein, we combine our experimental data with density functional theory (DFT) calculations and multivariate linear regression modeling to understand the structure-function relationships in phenazine-based mediated EET. These calculations demonstrate that the computed redox properties of phenazines in lipophilic environments (e.g., cell membrane) correlate to experimental mediated current densities. Additional DFT-derived molecular properties were considered to develop a predictive model, which could be used in metabolic engineering approaches to introduce phenazines as endogenous mediators into bacteria.

INTRODUCTION

Microbial electrochemical systems, using microorganisms as biological catalysts to convert chemical to electrical energy (Wang and Ren 2013), have gained significant interest in the past few decades as sustainable bioelectrochemical devices to address the continually increasing global energy demands (Bajracharya et al., 2016; Poizot and Dolhem 2011). They offer promise as technologies with several applications, such as environmental bioremediation and more energy-efficient wastewater treatments (Resch et al., 2008; Yang et al., 2012). In these bioelectrochemical systems, living microorganisms can transfer electrons through various extracellular electron transfer (EET) mechanisms to electronically conductive electrodes (e.g., typically anodes) (Pankratova and Gorton 2017; Pankratova et al., 2018). The microbe-electrode interaction is driven by complex oxidation-reduction (redox) reactions that occur during microbial respiration metabolism of abundant organic substances (Pankratova and Gorton 2017; Pankratova et al., 2018). The ability to promote a facile and efficient EET between microbes and electrodes is one of the major challenges in bioelectrocatalysis (Chen et al., 2020). As such, EET is a limiting factor in the development of advanced microbial electrochemical systems with enhanced power generation and improved overall performance (Chen et al., 2020; Kumar et al., 2017; Seviour and Hinks 2018).

In the context of EET in microorganisms, two main mechanisms have been proposed. One EET mechanism is direct electron transfer (DET), where electrode surfaces typically make physical contact with functional motifs, namely membrane-bound redox proteins (such as cytochrome c) on cellular surfaces, cellular pili, and/or nanowires that facilitate EET (Chen et al., 2020; Heydorn et al., 2020; Kumar et al., 2017; Schröder 2007; Seviour and Hinks 2018; Torres et al., 2010). The second EET mechanism is indirect mediated electron transfer (MET), where diffusive, soluble redox mediator systems act as electron shuttles between microorganisms and electrode surfaces (Chen et al., 2020; Kumar et al., 2017; Seviour and Hinks 2018). Most microbial species do not have redox-active proteins on the cellular surfaces to achieve DET with the exception of a few bacteria. Therefore, most microorganisms have MET-based mechanisms, which utilize electroactive mediator-based systems to enhance and/or achieve EET (Park and Zeikus 2000; Seviour and Hinks 2018). Specifically, bacteria that do not readily carry out EET, such as the model microorganism *Escherichia*

[1]Department of Chemistry, University of Utah, Salt Lake City, UT 84112, USA

[2]Center for Energy Science and Technology, Skolkovo Institute of Science and Technology, Bolshoi Boulevard 30 Bld. 1, Moscow 121205, Russia

[3]These authors contributed equally

[4]Lead contact

*Correspondence: olja.simoska@utah.edu (O.S.), minteer@chem.utah.edu (S.D.M.)

https://doi.org/10.1016/j.isci.2021.103033

coli, can chemically interact with conductive electrodes through the use of different soluble, diffusive electron mediators (Bennetto et al., 1983; Park and Zeikus 2000; Seviour and Hinks 2018), which can effectively enhance EET (Rau et al., 2002; Royer et al., 2002). In mediated microbial electrochemical systems, a suitable redox mediator should have an appropriate redox potential to link to the microbial respiration metabolism at play. Additionally, the electron mediator should be soluble and biologically compatible. Finally, the mediator should form a fast and reversible couple on the electrode surface, such that it is stable in both its oxidized and reduced forms. In addition to the commonly studied mediator systems employing quinones (Grattieri et al., 2018) and flavins (Marsili et al., 2008), several microbial electrochemical technologies have also demonstrated the use of phenazines as a redox mediator system to increase electron transfer rates (Rabaey et al., 2005; Seviour and Hinks 2018; Simoska et al. 2019b, 2021)

Phenazines constitute a group of redox-active secondary metabolites secreted by *Pseudomonas* species (Elliott et al., 2017; Simoska et al. 2019a, 2019b). These molecules have nitrogen-containing heterocyclic ring structures that differ based on the position and the nature of the functional group (Laursen and Nielsen 2004; Mavrodi et al. 2006, 2010; Pierson and Pierson 2010). Research studies have proposed and/or shown that phenazines can engage in redox cycling processes in which they can reduce molecular oxygen, causing the generation and accumulation of reactive oxygen species such as hydrogen peroxide and superoxide (Ahuja et al., 2008; Mavrodi et al., 2006; Pierson and Pierson 2010). The small size and similar physiological properties enable phenazine derivatives to facilitate electron transfer and cross-cellular membranes transferring content from cells to the extracellular environment (Glasser et al., 2014). Several studies have examined the impact of both naturally occurring as well as artificially synthesized phenazine derivatives on bacterial interaction and metabolism (Askitosari et al., 2019; Pierson and Pierson 2010; Simoska et al., 2021; Venkataraman et al., 2011). Additionally, phenazine-based redox mediators have been exogenously added to improve the overall performance of microbial electrochemical systems (Clifford et al., 2021; Simoska et al., 2021). For example, research has demonstrated that exogenously added phenazines improve electron transfer rates in microbial fuel cells (Rabaey et al., 2005). Namely, the use of phenazine-producing *Pseudomonas aeruginosa* in combination with exogenous phenazine mediators resulted in high electrical conductivity of biofilms on the electrode surface, which consequently enhanced the electricity generation from bacterial metabolism (Rabaey et al., 2005). While *P. aeruginosa* can self-produce endogenous electron shuttles via a complex regulatory phenazine biosynthetic pathway, highly pathogenic characteristics of *P. aeruginosa* strains limit the practical applications of phenazine-mediated microbial electrochemical systems using this microbe as the biocatalytic host (Askitosari et al., 2019; Venkataraman et al., 2011). Consequently, phenazines have been used as a mediator system in microbial bioelectrochemical systems with other non-pathogen microorganisms, such as obligate aerobic *Pseudomonas putida* (Askitosari et al., 2019; Schmitz et al., 2015), certain *E. coli* strains (Feng et al., 2018), and cyanobacterium *Synechocystis* sp. (Clifford et al., 2021).

The aim of this study is to build a library of suitable phenazine mediators and probe the structure-function properties for EET in *E. coli*. Recently, our research group reported a phenazine mediator system to promote EET from *E. coli* on carbon-based electrodes during glucose metabolism (Simoska et al., 2021). As a versatile model microorganism, gram-negative *E. coli* has been used as a biocatalyst in several microbial electrochemical systems (Chen et al., 2020; Glaven 2019; Jensen et al., 2010; Teravest et al., 2014; Wu et al., 2019). In addition to its fast growth rates and capability to oxidize a wide range of substrates (Fan and Song 2016), *E. coli* strains are non-pathogenic, making this microbe a versatile host for microbial-based bioelectrochemical applications. The respiration metabolism of *E. coli* can be used for bioelectrochemical purposes by adding exogenous electron mediators to the system. Our previous study experimentally evaluated distinct phenazine moieties as exogenous electron mediators to control EET in *E. coli*. The quantitative, electrochemical data showed distinctive mediated current densities based on the phenazine mediator structure and concentration. Additionally, these experimental results demonstrated that the rational design of mediated microbial EET systems is far more complicated than selecting a mediator with a suitable redox potential, which is the standard strategy for choosing a redox mediator.

Herein, we compare our previously reported experimental data on evaluating phenazine mediator performance with a detailed computational analysis based on density functional theory (DFT) calculations and multivariate linear regression (MLR) modeling to understand the structure-function relationships (e.g., structural and electronic properties) that control phenazine-mediated EET in *E. coli*. The redox reaction of phenazine mediators is considered to be a proton-coupled electron transfer mechanism (Elliott et al.,

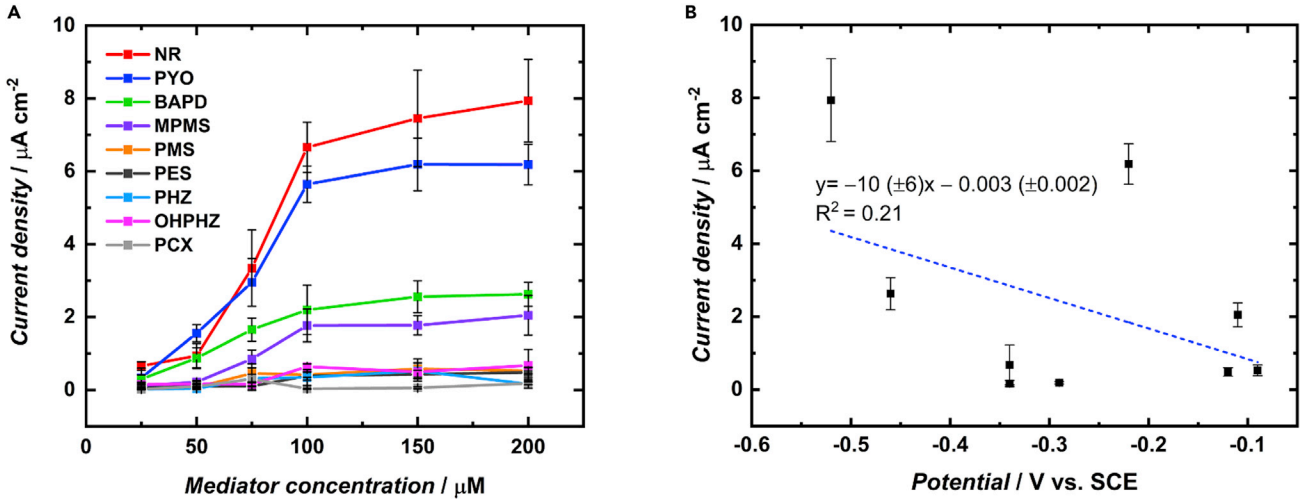

Figure 1. Experimentally determined mediated current densities as a function of phenazine mediator concentrations and experimentally determined mediated current densities as a function of the experimentally determined redox potential for each phenazine mediator

(A) Experimentally determined mediated current densities as a function of varying mediator concentrations for phenazine mediators, neutral red (NR) pyocyanin (PYO), benzo(A)phenazine-7,12-dioxide (BAPD), 1-methoxy-5-methylphenazinium methyl sulfate (MPMS), phenazine methosulfate (PMS), phenazine ethosulfate (PES), phenazine (PHZ), 1-hydroxyphenazine (OHPHZ), and phenazine-1-carboxamide (PCX), reported in our previous study (Simoska et al., 2021).

(B) Experimentally determined mediated current densities at 200 μM mediator concentration as a function of the experimentally measured redox potentials for each phenazine mediator. Error bars denote the standard deviations from n = 5.

2017; Huynh and Meyer 2007; Tan and Webster 2012), which is common in numerous biological and chemical processes. However, fundamental information about how phenazines are involved in microbial-based electron transfer processes remains very limited. Based on the differences in functional groups on the nitrogen-based heterocyclic core, phenazine derivatives have different physical and chemical properties. In this context, the position and nature of the distinct functional group can impact the redox potential, stability, and polarity (Mavrodi et al., 2006; Wang and Newman 2008) of phenazine mediators, thereby affecting the EET ability and mediated current outputs in microbial biocatalytic systems. Therefore, this study determines electronic and structural parameters to investigate fundamental processes of different phenazine forms that relate to the collection of electrons from *E. coli* paired with transport to and from the electrode surface. We identified the computationally derived properties of phenazine electrochemical mediators that correlate with measured mediated current densities, providing fundamental insights into the development of future mediated EET systems with improved kinetics.

RESULTS AND DISCUSSION

Mediated current densities in *E. coli* glucose metabolism

The ability to successfully establish an efficient EET between microorganisms and conductive electrode surfaces is one of the fundamental challenges in bioelectrocatalysis, specifically when rationally designing mediated microbial electrochemical systems. Our recent study described an experimental electrochemical characterization of different, soluble phenazines as exogenous redox mediators that facilitate EET from the model microorganism *E. coli* during glucose oxidation metabolism. The quantitative experimental electrochemical data resulted in distinct mediated current densities dependent on the phenazine mediator structure and concentration. A summary of the correlation between mediator concentrations for each phenazine and the mediated current density calculated from amperometric *i-t* tests is shown in Figure 1A. As reported in this recent study by our group (Simoska et al., 2021), minor changes in the phenazine-based mediator structures and concentrations resulted in notable differences in the mediated current outputs measured in *E. coli* consuming glucose, with 200 μM neutral red (NR) demonstrating the highest mediated current density (7.9 ± 0.9 μA cm^{-2}). We have now further evaluated data to determine if there is a possible correlation between the experimentally obtained formal redox potential of the different mediators in buffered aqueous media and the experimentally obtained mediated current densities (Figure 1B). It can be clearly noted that no apparent correlation (R^2 = 0.21) is found for the estimated formal redox potential for the

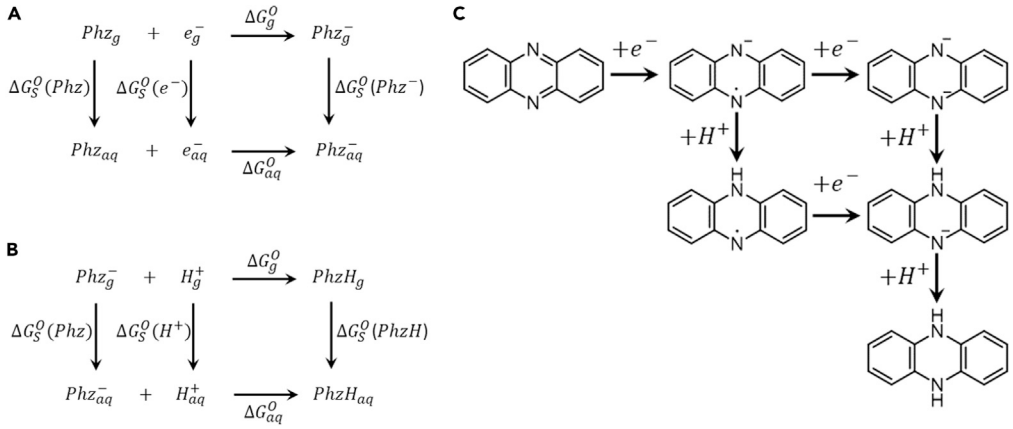

Figure 2. Thermodynamic cycles of electron and proton addition reactions for a phenazine

(A and B) Thermodynamic cycles of (A) electron and (B) proton addition reactions. *Phz* stands for a computed phenazine structure, with subscript *g* representing the gas phase and subscript *aq* representing the aqueous free energy structure generated.

(C) A representative square scheme mechanism for the two-electron, two-proton ($2e^-$, $2H^+$) reduction of phenazine (PHZ).

phenazine mediators measured by cyclic voltammetry in aqueous buffered media, which are displayed in Figure S1 in the supplemental information. Based on the result in Figure 1B, we sought to understand mediator performance in our system by correlating the experimental output of interest, specifically the mediated current density, to the electronic and structural parameters of each of the phenazine mediators evaluated. These data show that the aqueous solution-based redox potentials are not the single aspect controlling phenazine-mediated bioelectrocatalytic systems based on *E. coli* glucose metabolism. Therefore, we also considered a variety of factors describing the structural and electronic characteristics associated with the diffusion of phenazine mediators into and out of the membrane, such as hydrophobicity, hydrophilicity, and single-electron transfer steps understood to take place in the cell membrane. While previous research has demonstrated that, in certain cases, the mediator reduction potential does correlate to the increased mediated catalytic current responses (Hasan et al., 2015), our experimental results (Figure 1B) show that this explanation does not describe the experimental catalytic currents measured.

DFT calculation of formal reduction potentials of phenazine mediators

Our computational efforts based on DFT initially focused on correlating the computed with the experimentally derived mediator properties to ensure that geometry-optimized DFT structures accurately represent mediator species in solution. Thus, the electrochemical redox potentials from DFT-optimized structures were calculated referencing an established procedure (Chen et al., 2013; Ho et al., 2015; North et al., 2010; Rauschnot et al., 2009). In order to calculate the formal reduction potential, $E^{O'}$, for each of the phenazine mediators in the described training set, a thermodynamic cycle was used, as described in Figures 2A and 2B, to compute the $\Delta G^O_{reaction}$ for each electron and proton addition step. For these cycles, $\Delta G_S^O(e^-)$ is equal to the solvation energy of the electron (negligible, e.g., ~0 kcal mol^{-1}) (Bartmess 1994) and $\Delta G_S^O(H^+)$ is known and equal to the negative energy of a proton with a value of −264 kcal mol^{-1} (Camaioni and Schwerdtfeger 2005; Kelley et al., 2006; Tissandier et al., 1998). Each of these cycles was used in respective steps listed below, wherein each phenazine species undergoes two reversible electron transfers coupled with one or two proton additions, as illustrated in steps 1 through 4 or steps 1 through 3, respectively, following the square scheme mechanism depicted in Figure 2C. Therefore, to thoroughly describe these processes, these steps are generically listed as follows:

Step 1 $Phz + e^- \rightarrow Phz^{\bullet -}$

Step 2 $Phz^{\bullet -} + H^+ \rightarrow PhzH^{\bullet}$

Step 3 $PhzH^{\bullet} + e^- \rightarrow PhzH^-$

Step 4 $PhzH^- + H^+ \rightarrow PhzH_2$

Step 5 $Phz^{\bullet -} + e^- \rightarrow Phz^{2-}$

Step 6 $Phz^{2-} + H^+ \rightarrow PhzH^-$

Specifically of interest in aqueous-based systems (e.g., water), the reduction pathways are likely from oxidized phenazine to the one-electron, one-proton semi-phenazine (step 1 and 2 combined, $\Delta G^O(1e^- / 1H^+)$). Subsequently, this semi-phenazine may be reduced to the anionic, hydrogen-substituted phenazine (steps 1 through 3, $\Delta G^O(2e^- / 1H^+)$). This species may then be protonated, given the availability of a second hydrogen association site, to the fully reduced and protonated phenazine species (steps 1 through 4, $\Delta G^O(2e^- / 2H^+)$). With N-substituted phenazine mediators (except for PYO, which contains an oxo group to accept the second proton), the two-electron, two-proton ($2e^-$, $2H^+$) reduction is inaccessible. The Gibbs free energy of the reduction processes mentioned at standard state was then computed from the ground state structures of each of the phenazine mediators in the following manner:

$$\Delta G^O(1e^- / 1H^+) = \Delta G^O_{Step\ 1} + \Delta G^O_{Step\ 2} \quad \text{(Equation 1)}$$

$$\Delta G^O(2e^- / 1H^+) = \Delta G^O_{Step\ 1} + \Delta G^O_{Step\ 2} + \Delta G^O_{Step\ 3} \quad \text{(Equation 2)}$$

$$\Delta G^O(2e^- / 2H^+) = \Delta G^O_{Step\ 1} + \Delta G^O_{Step\ 2} + \Delta G^O_{Step\ 3} + \Delta G^O_{Step\ 4} \quad \text{(Equation 3)}$$

These Gibbs free energies were used to calculate the reduction potential for each reduction and protonation process through the Nernst equation:

$$E^O = -\frac{\Delta G^O(X)}{nF} - E^O_H \quad \text{(Equation 4)}$$

where E^O equals the standard reduction potential, $\Delta G^O(X)$ represents the Gibbs free energy of the reduction process of interest, n is the number of electrons transferred (here, 1 or 2 electrons), F is Faraday's constant with a value of 23.06 kcal mol^{-1} V^{-1}, and E^O_H is the normal hydrogen electrode potential with a value of 4.28 V as reported in previous literature (Kelley et al., 2006). These potentials were further converted to potentials versus saturated calomel electrode (SCE) by adding −241 mV. All DFT optimized structural coordinates and mediator-specific square schemes with energetically favored protonation sites can be found in Schemes S1–S9 provided in the supplemental information. Given the error present in calculations of pK_a values from DFT solvation models (Lian et al., 2018; Matsui et al., 2017; Orozco and Luque 2000) and perplexity surrounding specifics of reduction pathways for each phenazine mediator, a linear correlation was utilized to associate the likely processes in our system studied with our experimentally obtained results.

Given that the reduction of phenazine mediators occurs in 95% aqueous buffer solutions, these reduction reactions occur as a two-electron, two-proton ($2e^-$, $2H^+$) process at a specific pH (Elliott et al., 2017; Simoska et al., 2019b). Based on the CV data obtained at varying scan rates (see details in Figure S1 in the supplemental information) for each phenazine mediator in 20 mM MOPS buffer (pH 7) + 10 mM $MgCl_2$ + 100 mM glucose, the electrochemical behaviors of phenazines are not a purely reversible, outer-sphere electron transfer. These processes undergo quasi-reversible redox mechanisms (Elliott et al., 2017) that are dependent on the scan rate dependent with $\Delta E_p > 59$ mV/n. Generally, a phenazine redox couple may appear irreversible when the voltammetric experiments are performed at slow scan rates. However, at faster scan rates, the chemical reversibility of the system improves, as observed in the voltammetric data in Figure S1 in the supplemental information. It should be noted that, in certain cases, the phenazine redox event might also involve and follow on chemical reactions (such as EC mechanism) or adoptive steps, making it challenging to extract and/or estimate formal potentials. The peak anodic (i_{pa}) and peak cathodic (i_{pc}) current responses were plotted as a function of the square root of the different scan rates (see details in Figure S2 in the supplemental information). Since i_{pa} does not equal i_{pc} as described by the Randles-Sevcik equation (Bard and Faulkner 2000), the ratio of the peak anodic to peak cathodic current does not equal to 1 (see details for i_{pa}/i_{pc} for each phenazine listed in Table S1 in supplemental information), which further illustrates the quasi-reversible nature of phenazine redox processes.

The formal redox potentials for each phenazine were calculated and compared for experimental data. Figures 3A, 3B, and 3C show these results for the (a) one-electron, one-proton ($1e^-$, $1H^+$) reduction, (b) two-electron, one-proton ($2e^-$, $1H^+$) reduction, and (c) two-electron, two-proton ($2e^-$, $2H^+$) reduction (namely, ($2e^-$, $1H^+$) for the N-substituted phenazines), respectively, where the x axis represents the measured formal redox potential, and the y axis is the computed formal redox potential for phenazine mediators obtained

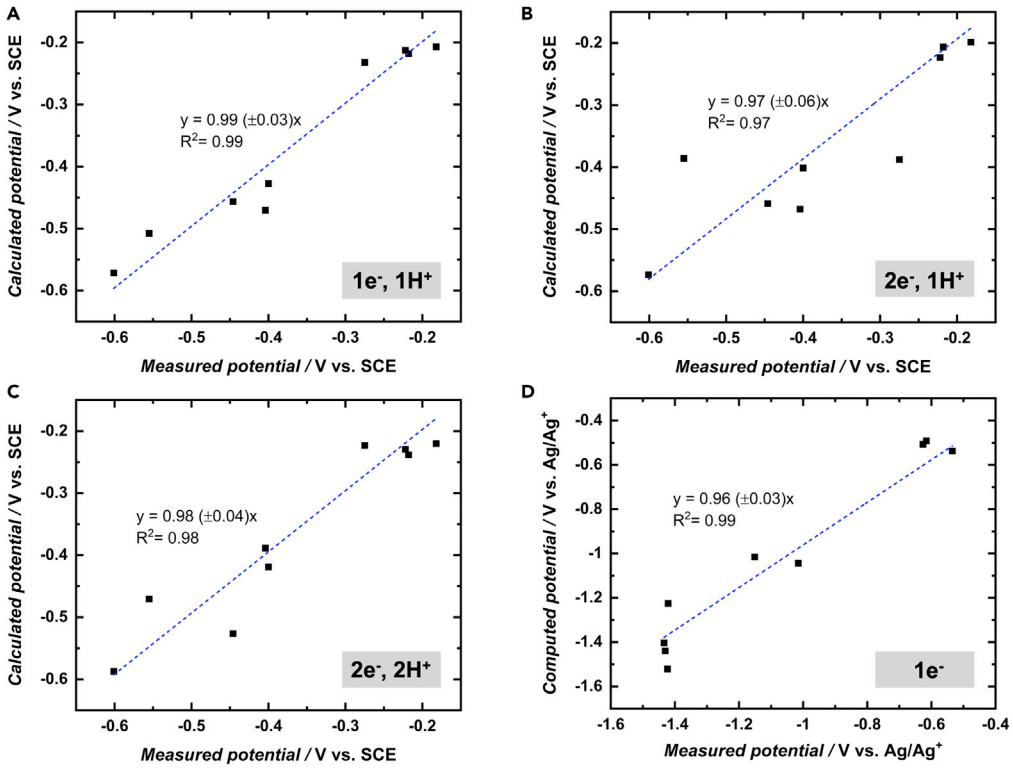

Figure 3. Computed formal reduction potentials vs. the measured formal redox potentials for the phenazine mediators set used in this study

(A–D) Computed formal reduction potentials as a function of the measured formal redox potentials for the phenazine mediators set for (A) one-electron, proton-coupled ($1e^-$, $1H^+$), (B) two-electron, proton-coupled ($2e^-$, $1H^+$), (C) two-electron, two-proton ($2e^-$, $2H^+$), and (D) single-electron, proton decoupled ($1e^-$) transfer processes. The experimentally measured formal redox potentials (vs. SCE) for phenazines in (A–C) were determined from cyclic voltammetry data of buffered aqueous-based media while the formal redox potentials (vs. Ag/Ag^+) for phenazines in (D) were obtained from cyclic voltammetry tests in aprotic media. The values for the measured formal redox potentials represent the average value from three replicates. Error bars are too small to be seen.

from DFT calculations (the computed phenazine mediator molecular atom coordinates are provided in Data S1). Interestingly, suitable linear correlations were observed between all three sets of computed formal reduction potentials for (1) the one-electron, one-proton ($1e^-$, $1H^+$) reduction with $R^2 = 0.99$, (2) the two-electron, one-proton ($2e^-$, $1H^+$) reduction with $R^2 = 0.97$, and (3) the two-electron, two-proton ($2e^-$, $2H^+$ or $1H^+$) reduction with $R^2 = 0.98$ to the experimentally determined formal potentials obtained from cyclic voltammetry experiments (see details in Figures S1 and S2 in the supplemental information), suggesting that these mediator redox processes may occur in aqueous media. These linear regression trends show that within the error, the calculated structures do match the geometry-based molecules present in aqueous solutions. Therefore, these reductive processes are all likely to occur either simultaneously or in succession in aqueous media, and the computed structures are all present in solution during electron transfer. Additionally, previous work by our research group (Grattieri et al., 2018), focusing on quinone-based mediators for generating biophotocurrent in photosynthetic purple microorganism *Rhodobacter capsulatus*, concluded that the redox behavior of mediators should be considered in aprotic environments (e.g., the lipophilic cell membrane) as it might play a critical role in electron transfer in mediated whole-cell systems. Therefore, the formal reduction potentials for the proton decoupled, single-electron ($1e^-$) transfer processes for each phenazine were also computed and experimentally determined using cyclic voltammetry experiments in aprotic media (see details in Figure S3 in the supplemental information). Figure 3D shows the correlation between the computed formal redox for the proton decoupled, single-electron transfer ($1e^-$) mechanism and the experimental voltammetric data for phenazine mediators in aprotic media. The excellent linear regression trend ($R^2 = 0.99$) observed suggests that within the error the computed phenazine structures match the phenazine molecules in aprotic solutions.

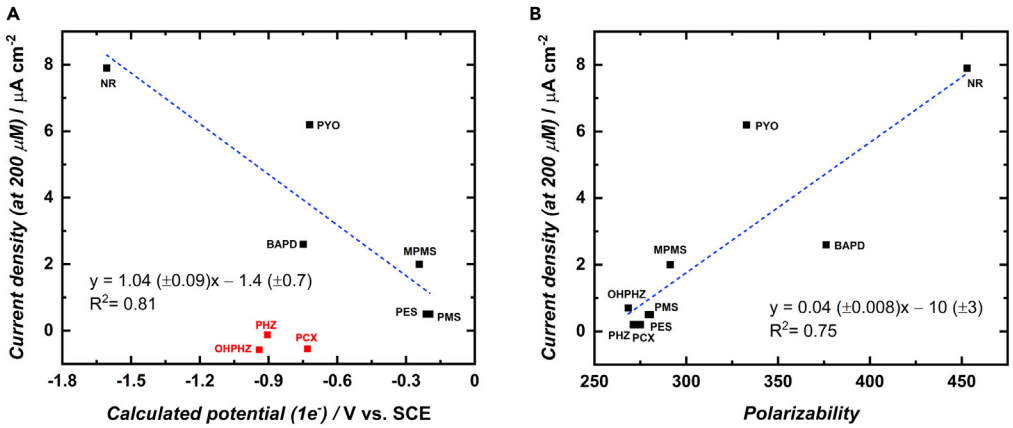

Figure 4. Experimentally determined mediated current densities at phenazine mediator concentration of 200 μM as a function of the calculated formal reduction potentials for the proton decoupled, single-electron ($1e^-$) transfer process and as a function of the mediator polarizability

(A) Experimentally determined mediated current densities at phenazine mediator concentration of 200 μM vs. computed potentials for the proton decoupled, single-electron ($1e^-$) transfer process for a set of six phenazine mediators. The three mediators (shown in red) that do not fit the proton decoupled, single-electron ($1e^-$) transfer process are shown.

(B) Mediated current densities at mediator concentration of 200 μM as a function of phenazine mediator polarizability for the entire set of nine phenazine mediator studies. The values and standard deviation for the mediated current densities are shown in Figure 1.

Multivariate linear regression modeling

To investigate the relationship between the structural properties and mediator performance of phenazines, additional factors were considered to describe the measured mediated current densities shown in Figure 1A. Namely, a parameter set of molecular properties (e.g., the formal reduction potential, polarity, lipophilicity, size, volume) derived from DFT and molecular mechanics (MM) was developed, and MLR analysis of each was performed using MATLAB software (MATLAB R2017b, 2017). Considering the possibility of the single-electron, proton decoupled ($1e^-$) process and the calculated formal reduction potentials as a universal descriptor yielded a direct linear correlation with catalytic current outputs (R^2 = 0.81), as shown in Figure 4A, for a subset of the phenazine mediators investigated, specifically NR, PYO, BAPD, MPMS, PMS, and PES. Single-electron ($1e^-$) processes are understood to occur in aprotic media (Figure 3D), which in our microbial-based bioelectrochemical system correspond to the cellular membrane. In this context, the observed correlation between mediated EET of *E. coli* and single-electron ($1e^-$) transfer processes for the subset of six exogenous phenazine mediators suggests that the limiting electron transfer step takes place in the lipophilic membrane of the bacterial cells, based on the linear correlation between the deprotonated, single-electron formal reduction potential correlation to observed mediated current outputs. It should be noted that when examining the whole data set of nine mediators, the formal reduction potential for the proton decoupled, single-electron ($1e^-$) steps is not a universal descriptor. Since this process describes only 70% of the mediators studied here, these results pointed to the need to consider additional factors for the full set of phenazine mediators tested.

Further efforts were made with the full set of parameters, namely descriptors associated with the mediator polarity, lipophilicity, size, and volume, obtained to develop a more appropriate model for the entire set of phenazine mediators studied. Analysis considering the computed standard deviation of the exact polarizability along x, y, and z axes (polarizability) of each mediator yielded a good univariate correlation to the experimentally determined mediated current densities (Figure 4B). When the polarizability is combined as a correcting factor to the single-electron ($1e^-$) formal reduction potential in a multivariate model, the three mediators (PCX, PHZ, and OHPHZ) that were excluded from the initial proton decoupled, single-electron ($1e^-$) model are included with a reasonable correlation (R^2 = 0.75) and leave-one-out internal validation (Q^2 = 0.61), as demonstrated in Figure 5A. However, the model is far more complex than the single descriptor polarizability model (Figure 4B) and does not improve the statistics or predictive power of the model. The pre-factor weighting also shows that the single-electron ($1e^-$) formal reduction potential is playing a minor role in the description of the mediated current density. Thus, other descriptors were

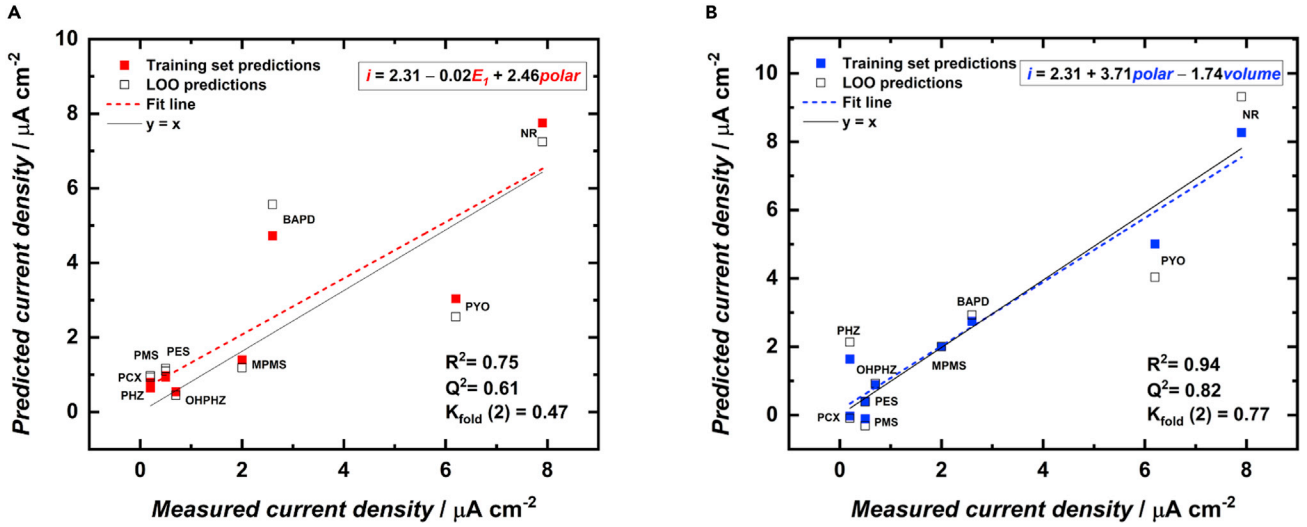

Figure 5. Multivariate linear regression models for the phenazine-mediated *E. coli*-based bioelectrochemical system

Multivariate linear regression models generated for the *E. coli* phenazine-mediated bioelectrochemical system showing mediated current densities as a function of the experimentally measured current densities for phenazines with descriptors.

(A) A bivariate model with the single-electron ($1e^-$) formal potential (E_1) and polarizability (*polar*) correlated to the mediated current output, *i*.

(B) Final model correlating the polarizability (*polar*) and molar volume (*volume*) descriptors with the mediated current outputs (*i*). In both (A) and (B), Q^2 represents the statistics associated with leave-one-out analysis and K_{fold} characterizes the cross-validation statistics. Equations are given for each model, where *i* is the current density, E_1 is the computed formal reduction potential (V vs. SCE) for the single-electron ($1e^-$) process, *polar* is the standard deviation of the polarizability, and *volume* is the molar volume ($Bohr^3\ mol^{-1}$).

introduced in our parameter set to pair with the polarizability term to generate a more predictive model, limiting our search to bivariate models to avoid overfitting as the full training set contains nine values. An excellent bivariate model was isolated that includes the polarizability with the molar volume as parameters, both of which were obtained through DFT. This model and its corresponding statistics, shown in Figure 5B, illustrate that the more polarizable a phenazine mediator and the smaller the molar volume, the greater the current enhancement. Thus, our hypothesis that electron transfer occurs in the lipophilic environment of the cell membrane proved to be only partially correct as the pre-factor weighting of normalized descriptor values in the model demonstrates that there are other factors of greater predictive power to describe the mediated current densities in this *E. coli*-based system. It is interesting to note that modeling parameters that are directly associated with lipophilicity and transport into or through the cell membrane did not show a direct correlation with the mediated current densities. However, descriptors for mediator polarizability and size showed promise, which is explained in the subsequent discussion.

To rationalize this model, the polarizability factor describes the distortion of the electron cloud in an electric field, which could be induced by electrodes, ions, and other highly charged system constituents. Isotropic polarizability, further, is the average or the molecule's polarizability in the x, y, and z directions. Therefore, the standard deviation of this value gives a quantitative measure to the relative similarity in polarizability between the x, y, and z terms. The model suggests that the greater the polarizability deviation, the better the mediator performance is. A possible explanation for this result is that the association of the phenazine with the cell membrane requires transport through a highly charged environment (e.g., extracellular ions involved in membrane potential, phosphate heads on phospholipids) before entering the aprotic environment within the lipid bilayer. Furthermore, *E. coli* as gram-negative bacteria are characterized by high densities of lipopolysaccharides in the outer leaflet of the cell membrane, increasing the negative charge density on the outer surface of the cell. Consequently, a more polarizable molecule would be conducted to the bilayer through this highly charged hydrophilic environment to finally participate in charge transfer within the hydrophobic interior of the cell membrane.

The molar volume is a measure of the molecule's molar mass divided by its density in a standard state. Thus, this parameter essentially describes the ability of the molecule to pack into a given space. This is loosely related to the solvent cavity volume (in our system) as well as the molecular weight (without counter ions

present), providing a steric parameter for the model. The model notes that as the molar volume decreases, the mediator performance is enhanced, which suggests that the molecule can move more easily through a medium with a smaller solvent shell and pack more closely with itself and similarly structured molecules. As such, this factor essentially describes not only how large the molecule is sterically but also how it moves through the solution with its hydration shell. Therefore, molar volume as a parameter also points to the facility of transport to and from the lipophilic region of the cell membrane as a major contributing factor in the phenazine mediator performance (see details in Figure S4 the supplemental information). These characteristics must be considered when selecting and/or designing a mediator that will result in the optimal current outputs for a given phenazine-mediated microbial bioelectrochemical system. Without external validation of the data points, the model's predictive power should be used with caution. Specifically, future studies need to validate the performance of the current model in more complex biological scenarios where variations in environmental parameters including pH, O_2 levels, temperature, concentrations of glucose (and other carbon-based sources), and the potential presence of other competing redox molecules need to be considered in the performance of phenazine-based mediated microbial bioelectrochemical systems. These physicochemical parameters should be meticulously analyzed with regard to how they impact the mediated current densities and also to validate the present model and/or generate a new, multifaceted model based on the one presented in this study. Further experimental investigations are necessary to elucidate the limiting transport kinetics of the bulk solutions and phenazine electrochemical mediator, which is a subject of further research. Finally, future efforts need to identify any specific enzymes in the metabolism of *E. coli* that might participate in phenazine reduction processes and their location in *E. coli* cells as it has previously been demonstrated in *P. aeruginosa* cells (Chukwubuikem et al., 2021; Glasser et al., 2017; Jo et al., 2020; Price-Whelan et al., 2007).

At present, the predictive model with good statistics provides a means to discover new phenazine-based mediators for further enhancement of the electron harvesting efficiency of the studied system. Specifically, the model can be utilized to predict mediator performance of both naturally occurring (e.g., PYO, OHPHZ, PCX) as well as artificially synthesized phenazines (e.g., BAPD, MPMS, PMS, PES, PHZ, NR). Additionally, this model can be used to predict the mediated current outputs for the naturally occurring phenazines in the complex regulatory *P. aeruginosa* biosynthetic pathway that are not commercially available due to their highly reactive natures, such as 5-methylphenazine-1-carboxylic acid (5-MCA) (Simoska et al. 2019a, 2019b). To demonstrate the applicability of this predictive model, the expected value for the current density of highly reactive 5-MCA was calculated to be 1.6 $\mu A\ cm^{-2}$. Therefore, this model could successfully be employed to predict the expected mediated current densities for bioelectrochemical systems utilizing other phenazine mediators with similar unstable nature to 5-MCA. This model provides critical insights into synthetic biology strategies and metabolic and genetic manipulation approaches to engineer various *E. coli* strains, not only with the phenazine biosynthetic pathway but also with incorporating novel and specifically engineered enzymes, to self-produce phenazine mediators of interest that will result in optimal current outputs in microbial electrochemical systems. Thus, this model is important for designing better performing mediated microbial bioelectrochemical systems with optimal and enhanced current outputs that have various applications ranging from more energy-efficient wastewater treatments, environmental bioremediation, and the synthesis of value-added products.

The rational design of mediated microbial bioelectrocatalytic systems with enhanced current density is far more complex than only choosing a mediator with an adequate redox potential, requiring an in-depth consideration of the fundamental bioelectrochemical reactions controlling EET. This study shows that special considerations are necessary for the advancement of redox mediator systems for model microorganism *E. coli*. The MLR correlation between the experimental phenazine-mediated current densities in *E. coli* and computed molecular characteristics indicates that the redox mechanisms of phenazine mediators need to be carefully evaluated not only in an aqueous buffer as the electrolyte solution but also in an aprotic environment representative of the cell membrane of bacteria. Specifically, our computational findings provide critical insight into describing aspects of the EET mechanism in *E. coli*, suggesting that a subset of the soluble phenazine mediators evaluated undergo proton decoupled, single-electron ($1e^-$) transfer steps. Furthermore, we considered additional factors, including polarizability and molar volume of phenazine mediators, to develop a more appropriate model with the entire set of phenazine mediators. The findings demonstrate that the polarizability standard deviation and molar volume parameters are major contributing factors to the phenazine performance with regard to the ability of transport to/from the lipophilic region of the cell membrane. Therefore, all these characteristics need to be considered when designing

mediator systems to develop phenazine-mediated microbial biocatalytic systems with enhanced performances. The model and statistic described in this study can thus be used as a predictive model to achieve this critical task to design future microbial-based mediated EET systems.

Limitations of the study

There are limitations of this study that should be considered when extending the model to other microbial electrochemical systems where microbes other than *Escherichia coli*, such as *Pseudomonas aeruginosa*, and *Pseudomonas putida* are used as the microbial biocatalytic host. Specific enzymes that might participate in phenazine reduction processes might differ from one microorganism to another due to distinct metabolic pathways. While *E. coli* is the most common model microorganism, *P. aeruginosa* is pathogenic species with other additional metabolic and quorum sensing pathways and *P. putida* is an obligate aerobe species (requires O_2) that has limitations to be used as a microbe in the anaerobic (O_2-free) anodic chamber in microbial electrochemical systems. These specific differences in metabolism between microorganism species will impact the reduction processes of phenazine mediators used to facilitate electron transfer. Therefore, additional experimental microorganisms need to be tested with the predictive model before we can have confidence in the applicability of our model to other microbe species. Further external validation points are necessary to evaluate the predictive mediated current density model with additional environmental factors, including pH, temperature, and O_2, which could all impact the electrochemical properties and electron transfer of the mediators in a given microbial electrochemical system.

STAR★METHODS

Detailed methods are provided in the online version of this paper and include the following:

- KEY RESOURCE TABLE
- RESOURCE AVAILABILITY
  - Lead contact
  - Materials availability
  - Data and code availability
- METHOD DETAILS
  - Chemicals
  - Phenazine mediator preparation
  - Electrochemical setup
  - Density functional theory
  - Multivariate linear regression modeling

SUPPLEMENTAL INFORMATION

Supplemental information can be found online at https://doi.org/10.1016/j.isci.2021.103033.

ACKNOWLEDGMENTS

The authors acknowledge funding for this study that was provided by the Office of Naval Research (ONR) grant N000142114008. O.S. is supported and funded by the 2020-2022 Irving S. Sigal Postdoctoral Fellowship from the American Chemical Society. The support and resources from the Center for High Performance Computing at the University of Utah are gratefully acknowledged. Z.R. and O.S. thank Erin Gaffney and Dr. Matthew Prater for helpful discussion points.

AUTHOR CONTRIBUTIONS

Z. R. and O.S. contributed equally to the work. O.S. and S.D.M. conceived the study. Z.R. and O.S. designed the study, experiments, and computations. Z.R. performed all computational calculations. O.S. performed all experimental components to this work. A.D. assisted O.S. with collecting cyclic voltammetry data in aprotic media. Z.R., O.S., K.J.S., and S.D.M. analyzed the data and results. K.J.S. provided intellectual input and valuable advice for this work. O.S. and Z.R. wrote the paper. All authors contributed to editing and have given approval of final version of the manuscript. S.D.M. supervised and administered funding for the research.

DECLARATION OF INTERESTS

The authors declare no competing interests.

Received: June 3, 2021
Revised: July 19, 2021
Accepted: August 20, 2021
Published: September 24, 2021

REFERENCES

Ahuja, E.G., Janning, P., Mentel, M., Graebsch, A., Breinbauer, R., Hiller, W., Costisella, B., Thomashow, L.S., Mavrodi, D.V., and Blankenfeldt, W. (2008). PhzA/B catalyzes the formation of the tricycle in phenazine biosynthesis. J. Am. Chem. Soc. *130*, 17053–17061.

Askitosari, T.D., Boto, S.T., Blank, L.M., and Rosenbaum, M.A. (2019). Boosting heterologous phenazine production in *Pseudomonas putida* KT2440 through the exploration of the natural sequence space. Front. Microbiol. *10*, 1990.

Bajracharya, S., Sharma, M., Mohanakrishna, G., Dominguez Benneton, X., Strik, D.P.B.T.B., Sarma, P.M., and Pant, D. (2016). An overview on emerging bioelectrochemical systems (BESs): technology for sustainable electricity, waste remediation, resource recovery, chemical production and beyond. Renew. Energy *98*, 153–170.

Bard, A.J., and Faulkner, L.R. (2000). Electrochemical Methods: Fundamentals and Applications (Wiley).

Bartmess, J.E. (1994). Thermodynamics of the electron and the proton. J. Phys. Chem. *98*, 6420–6424.

Bennetto, H.P., Stirling, J.L., Tanaka, K., and Vega, C.A. (1983). Anodic reactions in microbial fuel cells. Biotechnol. Bioeng. *25*, 559–568.

Camaioni, D.M., and Schwerdtfeger, C.A. (2005). Comment on "accurate experimental values for the free energies of hydration of H^+, OH^-, and H_3O^+". J. Phys. Chem. A. *109*, 10795–10797.

Chen, H., Simoska, O., Lim, K., Grattieri, M., Yuan, M., Dong, F., Lee, Y.S., Beaver, K., Weliwatte, S., Gaffney, E.M., and Minteer, S.D. (2020). Fundamentals, applications, and future directions of bioelectrocatalysis. Chem. Rev. *120*, 12903–12993.

Chen, J.J., Chen, W., He, H., Li, D.B., Li, W.W., Xiong, L., and Yu, H.Q. (2013). Manipulation of microbial extracellular electron transfer by changing molecular structure of phenazine-type redox mediators. Environ. Sci. Technol. *47*, 1033–1039.

Chukwubuikem, A., Berger, C., Mady, A., and Rosenbaum, M.A. (2021). Role of phenazine-enzyme physiology for current generation in a bioelectrochemical system. Microb. Biotechnol. *14*, 1613–1626.

Clifford, E.R., Bradley, R.W., Wey, L.T., Lawrence, J.M., Chen, X., Howe, C.J., and Zhang, J.Z. (2021). Phenazines as model low-midpoint potential electron shuttles for photosynthetic bioelectrochemical systems. Chem. Sci. *12*, 3328–3338.

Elliott, J., Simoska, O., Karasik, S., Shear, J.B., and Stevenson, K.J. (2017). Transparent carbon ultramicroelectrode arrays for the electrochemical detection of a aacterial warfare toxin, pyocyanin. Anal. Chem. *89*, 6285–6289.

Fan, L.-P., and Song, X. (2016). Overview on electricigens for microbial fuel cell *10*, 398–406.

Feng, J., Qian, Y., Wang, Z., Wang, X., Xu, S., Chen, K., and Ouyang, P. (2018). Enhancing the performance of Escherichia coli-inoculated microbial fuel cells by introduction of the phenazine-1-carboxylic acid pathway. J. Biotechnol. *275*, 1–6.

Frisch, M.J., Trucks, G.W., Schlegel, H.B., Scuseria, G.E., Robb, M.A., Cheeseman, J.R., Scalmani, G., Barone, V., Petersson, G.A., Nakatsuji, H., et al. 2016. Gaussian 16 Rev. C.01. Wallingford, CT.

Glasser, N.R., Kern, S.E., and Newman, D.K. (2014). Phenazine redox cycling enhances anaerobic survival in *Pseudomonas aeruginosa* by facilitating generation of ATP and a proton-motive force. Mol. Microbiol. *92*, 399–412.

Glasser, N.R., Wang, B.X., Hoy, J.A., and Newman, D.K. (2017). The pyruvate and alpha-ketoglutarate dehydrogenase complexes of *Pseudomonas aeruginosa* catalyze pyocyanin and phenazine-1-carboxylic acid reduction via the subunit dihydrolipoamide dehydrogenase. J. Biol. Chem. *292*, 5593–5607.

Glaven, S.M. (2019). Bioelectrochemical systems and synthetic biology: more power, more products. Microb. Biotechnol. *12*, 819–823.

Grattieri, M., Rhodes, Z., Hickey, D.P., Beaver, K., and Minteer, S.D. (2018). Understanding biophotocurrent generation in photosynthetic purple bacteria. ACS Catal. *9*, 867–873.

Guo, J.-Y., Minko, Y., Santiago, C.B., and Sigman, M.S. (2017). Developing comprehensive computational parameter sets to describe the performance of pyridine-oxazoline and related ligands. ACS Catal. *7*, 4144–4151.

Hariharan, P.C., and Pople, J.A. (1973). The influence of polarization functions on molecular orbital hydrogenation energies. Theor. Chim. Acta *28*, 213–222.

Hasan, K., Reddy, K.V.R., Eßmann, V., Gořecki, K., Conghaile, P.O., Schuhmann, W., Leech, D., HagErhalL, C., and Gorton, L. (2015). Electrochemical communication between electrodes and *Rhodobacter capsulatus* grown in different metabolic modes. Electroanalysis *27*, 118–127.

Hehre, W.J., Ditchfield, R., and Pople, J.A. (1972). Self-consistent molecular orbital methods. XII. Further extensions of Gaussian-type basis sets for use in molecular orbital studies of organic molecules. J. Chem. Phys. *56*, 2257.

Heydorn, R.L., Engel, C., Krull, R., and Dohnt, K. (2020). Strategies for the targeted Improvement of anodic electron transfer in microbial fuel cells. ChemBioEng Rev. *7*, 4–17.

Ho, J., Coote, M.L., Cramer, C.J., and Truhlar, D.G. (2015). Theoretical Calculation of Reduction Potentials. Organic Electrochemistry: Revised and Expanded. 5th ed. (CRC Press, Taylor and Francis Group).

Huynh, M.H.V., and Meyer, T.J. (2007). Proton-coupled electron transfer. Chem. Rev. *107*, 5004–5064.

Jensen, H.M., Albers, A.E., Malley, K.R., Londer, Y.Y., Cohen, B.E., Helms, B.A., Weigele, P., Groves, J.T., and Ajo-Franklin, C.M. (2010). Engineering of a synthetic electron conduit in living cells. Proc. Natl. Acad. Sci. U S A. *107*, 19213–19218.

Jo, J., Price-Whelan, A., Cornell, W.C., and Dietrich, L.E.P. (2020). Interdependency of respiratory metabolism and phenazine-associated physiology in *Pseudomonas aeruginosa* PA14. J. Bacteriol. *202*, e00700–e00719.

Kelley, C.P., Cramer, C.J., and Truhlar, D.G. (2006). Aqueous solvation free energies of ions and ion−water clusters based on an accurate value for the absolute aqueous solvation free energy of the proton. J. Phys. Chem. B *110*, 16066–16081.

Kumar, A., Hsu, L.H.-H., Kavanagh, P., Barrière, F., Lens, P.N.L., Lapinsonnière, L., Lienhard, V.J.H., Schröder, U., Jiang, X., and Leech, D. (2017). The ins and outs of microorganism–electrode electron transfer reactions. Nat. Rev. Chem. *1*, 0024.

Laursen, J.B., and Nielsen, J. (2004). Phenazine natural products: biosynthesis, synthetic analogues, and biological activity. Chem. Rev. *104*, 1663–1686.

Lian, P., Johnston, R.C., Parks, J.M., and Smith, J.C. (2018). Quantum chemical calculation of p*Ka*s of environmentally relevant functional groups: carboxylic acids, amines, and thiols in aqueous solution. J. Phys. Chem. A. *122*, 4366–4374.

Marenich, A.V., Cramer, C.J., and Truhlar, D.G. (2009a). Performance of SM6, SM8, and SMD on the SAMPL1 test set for the prediction of small-molecule solvation free energies. J. Phys. Chem. B *113*, 4538–4543.

Marenich, A.V., Cramer, C.J., and Truhlar, D.G. (2009b). Universal solvation model based on solute electron density and on a continuum model of the solvent defined by the bulk dielectric constant and atomic surface tensions. J. Phys. Chem. B *113*, 6378–6396.

Marsili, E., Baron, D.B., Shikhare, I.D., Coursolle, D., Gralnick, J.A., and Bond, D.R. (2008). *Shewanella* secretes flavins that mediate extracellular electron transfer. Proc. Natl. Acad. Sci. U S A. *105*, 3968–3973.

MATLAB R2017b. 2017. Natick: MA: Mathworks, I.

Matsui, T., Shigeta, Y., and Morihashi, K. (2017). Assessment of methodology and chemical group dependences in the calculation of the p*Ka* for several chemical groups. J. Chem. Theor. Comput. *13*, 4791–4803.

Mavrodi, D.V., Blankenfeldt, W., and Thomashow, L.S. (2006). Phenazine compounds in fluorescent *Pseudomonas* spp. biosynthesis and regulation. Annu. Rev. Phytopathol. *44*, 417–445.

Mavrodi, D.V., Peever, T.L., Mavrodi, O.V., Parejko, J.A., Raaijmakers, J.M., Lemanceau, P., Mazurier, S., Heide, L., Blankenfeldt, W., Weller, D.M., and Thomashow, L.S. (2010). Diversity and evolution of the phenazine biosynthesis pathway. Appl. Environ. Microbiol. *76*, 866–879.

North, M.A., Bhattacharyya, S., and Truhlar, D.G. (2010). Improved density functional description of the electrochemistry and structure−property descriptors of substituted flavins. J. Phys. Chem. B *114*, 14907–14915.

Orozco, M., and Luque, F.J. (2000). Theoretical methods for the description of the solvent effect in biomolecular systems. Chem. Rev. *11*, 4187–4226.

Pankratova, G., and Gorton, L. (2017). Electrochemical communication between living cells and conductive surfaces. Curr. Opin. Electrochem. *5*, 193–202.

Pankratova, G., Leech, D., Gorton, L., and Hederstedt, L. (2018). Extracellular electron transfer by the gram-positive bacterium *Enterococcus faecalis*. Biochemistry *57*, 4597–4603.

Park, D.H., and Zeikus, J.G. (2000). Electricity generation in microbial fuel cells using neutral red as an electronophore. Appl. Environ. Microbiol. *66*, 1292–1297.

Pierson, L.S., 3rd, and Pierson, E.A. (2010). Metabolism and function of phenazines in bacteria: impacts on the behavior of bacteria in the environment and biotechnological processes. Appl. Microbiol. Biotechnol. *86*, 1659–1670.

Poizot, P., and Dolhem, F. (2011). Clean energy new deal for a sustainable world: from non-CO_2 generating energy sources to greener electrochemical storage devices. Energy Environ. Sci. *4*, 2003–2019.

Price-Whelan, A., Dietrich, L.E., and Newman, D.K. (2007). Pyocyanin alters redox homeostasis and carbon flux through central metabolic pathways in *Pseudomonas aeruginosa* PA14. J. Bacteriol. *189*, 6372–6381.

Rabaey, K., Boon, N., Hofte, M., and Verstraete, W. (2005). Microbial phenazine production enhances electron transfer in biofuel cells. Environ. Sci. Technol. *39*, 3401–3408.

Rau, J., Knackmuss, H.J., and Stolz, A. (2002). Effects of different quinoid redox mediators on the anaerobic reduction of azo dyes by bacteria. Environ. Sci. Technol. *36*, 1497–1504.

Rauschnot, J.C.J., Yang, C., Yang, V., and Bhattacharyya, S. (2009). Theoretical determination of the redox potentials of NRH:quinone oxidoreductase 2 using quantum mechanical/molecular mechanical simulations. J. Phys. Chem. B *113*, 8149–8157.

Resch, G., Held, A., Faber, T., Panzer, C., Toro, F., and Haas, R. (2008). Potentials and prospects for renewable energies at global scale. Energy Policy *36*, 4048–4056.

Royer, R.A., Burgos, W.D., Fisher, A.S., Unz, R.F., and Dempsey, B.A. (2002). Enhancement of biological reduction of hematite by electron shuttling and Fe(II) complexation. Environ. Sci. Technol. *36*, 1939–1946.

Santiago, C.B., Guo, J.Y., and Sigman, M.S. (2018). Predictive and mechanistic multivariate linear regression models for reaction development. Chem. Sci. *9*, 2398–2412.

Schmitz, S., Nies, S., Wierckx, N., Blank, L.M., and Rosenbaum, M.A. (2015). Engineering mediator-based electroactivity in the obligate aerobic bacterium *Pseudomonas putida* KT2440. Front. Microbiol. *6*, 284.

Schröder, U. (2007). Anodic electron transfer mechanisms in microbial fuel cells and their energy efficiency. Phys. Chem. Chem. Phys. *9*, 2619–2629.

Schrödinger Release 2021-2: QikProp. 2021. New York: NY: Schrödinger, LLC.

Seviour, T.W., and Hinks, J. (2018). Bucking the current trend in bioelectrochemical systems: a case for bioelectroanalytics. Crit. Rev. Biotechnol. *38*, 634–646.

Sigman, M.S., Harper, K.C., Bess, E.N., and Milo, A. (2016). The development of multidimensional analysis tools for asymmetric catalysis and beyond. Acc. Chem. Res. *49*, 1292–1301.

Simoska, O., Gaffney, E.M., Lim, K., Beaver, K., and Minteer, S.D. (2021). Understanding the properties of phenazine mediators that promote extracellular electron transfer in *Escherichia coli*. J. Electrochem. Soc. *168*, 025503.

Simoska, O., Sans, M., Eberlin, L.S., Shear, J.B., and Stevenson, K.J. (2019a). Electrochemical monitoring of the impact of polymicrobial infections on *Pseudomonas aeruginosa* and growth dependent medium. Biosens. Bioelectron. *142*, 111538.

Simoska, O., Sans, M., Fitzpatrick, M.D., Crittenden, C.M., Eberlin, L.S., Shear, J.B., and Stevenson, K.J. (2019b). Real-time electrochemical detection of *Pseudomonas aeruginosa* phenazine metabolites using transparent carbon ultramicroelectrode arrays. ACS Sens *4*, 170–179.

Tan, S.L., and Webster, R.D. (2012). Electrochemically induced chemically reversible proton-coupled electron transfer reactions of riboflavin (vitamin B2). J. Am. Chem. Soc. *134*, 5954–5964.

Teravest, M.A., Zajdel, T.J., and Ajo-Franklin, C.M. (2014). The Mtr pathway of *Shewanella oneidensis* MR-1 couples substrate utilization to current production in *Escherichia coli*. ChemElectroChem *1*, 1874–1879.

Tissandier, M.D., Cowen, K.A., Feng, W.Y., Gundlach, E., Cohen, M.H., Earhart, A.D., Coe, J.V., and Tuttle, T.R. (1998). The proton's absolute aqueous enthalpy and gibbs free energy of solvation from cluster-ion solvation data. J. Phys. Chem. A. *102*, 7787–7794.

Torres, C.I., Marcus, A.K., Lee, H.S., Parameswaran, P., Krajmalnik-Brown, R., and Rittmann, B.E. (2010). A kinetic perspective on extracellular electron transfer by anode-respiring bacteria. FEMS Microbiol. Rev. *34*, 3–17.

Venkataraman, A., Rosenbaum, M.A., Perkins, S.D., Werner, J.J., and Angenent, L.T. (2011). Metabolite-based mutualism between *Pseudomonas aeruginosa* PA14 and *Enterobacter aerogenes* enhances current generation in bioelectrochemical systems. Energy Environ. Sci. *4*, 4550–4559.

Wang, H., and Ren, Z.J. (2013). A comprehensive review of microbial electrochemical systems as a platform technology. Biotechnol. Adv. *31*, 1796–1807.

Wang, Y., and Newman, D.K. (2008). Redox reactions of phenazine antibiotics with ferric (hydr)oxides and molecular oxygen. Environ. Sci. Technol. *42*, 2380–2386.

Weigend, F., and Ahlrichs, R. (2005). Balanced basis sets of split valence, triple zeta valence and quadruple zeta valence quality for H to Rn: design and assessment of accuracy. Phys. Chem. Chem. Phys. *7*, 3297–3305.

Wu, Z., Wang, J., Liu, J., Wang, Y., Bi, C., and Zhang, X. (2019). Engineering an electroactive *Escherichia coli* for the microbial electrosynthesis of succinate from glucose and CO_2. Microb. Cell Fact. *18*, 15.

Yang, Y., Xu, M., Guo, J., and Sun, G. (2012). Bacterial extracellular electron transfer in bioelectrochemical systems. Process. Biochem. *47*, 1707–1714.

Zhao, Y., and Truhlar, D.G. (2008a). Density functionals with broad applicability in chemistry. Acc. Chem. Res. *41*, 157–167.

Zhao, Y., and Truhlar, D.G. (2008b). The M06 suite of density functionals for main group thermochemistry, thermochemical kinetics, noncovalent interactions, excited states, and transition elements: two new functionals and systematic testing of four M06-class functionals and 12 other functionals. Theor. Chem. Acc. *120*, 215–241.

STAR★METHODS

KEY RESOURCE TABLE

REAGENT or RESOURCE	SOURCE	IDENTIFIER
Bacterial and virus strains		
Escherichia coli BL21	New England BioLabs	C2530H
Chemicals, peptides, and recombinant proteins		
D-glucose	Fisher Scientific Inc	D16-500; CAS: 50-99-7
Magnesium chloride	Fisher Scientific Inc	BP214-500; CAS: 7786-30-3
3-(N-morpholino)propane sulfonic acid	Sigma-Aldrich	M1254; CAS: 1132-61-2
N,N-dimethylformamide (anhydrous, 99.8%)	Sigma-Aldrich	227056; CAS: 68-12-2
Ethanol	Sigma-Aldrich	459836; CAS: 64-17-5
Tetrabutylammonium hexafluorophosphate	Sigma-Aldrich	86879; CAS: 3109-63-5
Phenazine	Sigma-Aldrich	P13207; CAS: 92-82-0
Neutral red	Sigma-Aldrich	N4638; CAS: 553-24-2
Phenazine ethosulfate	Sigma-Aldrich	P4544; CAS: 10510-77-7
Phenazine methosulfate	Sigma-Aldrich	P9625; CAS: 299-11-6
Phenazine-1-carboxamide	Sigma-Aldrich	SY3H3249FA6D; CAS: 550-89-0
Benzo(A)phenazine-7,12-dioxide	Sigma-Aldrich	R415219; CAS: 18636-88-9
1-Hydroxyphenazine	Cayman Chemical	28064; CAS: 528-71-2
Pyocyanin	Cayman Chemical	10009594; CAS: 85-66-5
1-Methoxy-5-methylphenazinimum methyl sulfate	Cayman Chemical	21258; CAS: 65162-13-2
Software and algorithms		
Gaussian16	Gaussian, Inc.	https://gaussian.com/
Python 3	Python Software Foundation	https://www.python.org/
MATLAB 2018	The MathWorks, Inc.	https://www.mathworks.com/
MacroModel	Schrödinger, Inc.	https://www.schrodinger.com/
OriginPro 2019b	OriginLab Corporation	https://www.originlab.com/2019b

RESOURCE AVAILABILITY

Lead contact

Further information and requests for resources and reagents should be directed to and will be fulfilled by the Lead Contact, S. D. Minteer (minteer@chem.utah.edu).

Materials availability

This study did not generate unique reagents. Requests for samples that were analyzed in this study can be directed to the Lead Contact, S. D. Minteer (minteer@chem.utah.edu).

Data and code availability

This paper did not generate and does not report original code. The code and software used for computations in this study are described in the method details and the key resource table. The experimental details regarding the measured mediated current densities used for modeling in this work are described in our previous study (Simoska et al., 2021). Any additional information required to analyze the data reported in this paper is available from the Lead Contact, S. D. Minteer (minteer@chem.utah.edu), upon request.

METHOD DETAILS

Chemicals

All reagents and chemicals were used as received. 1-Methoxy-5-methylphenazinimum methyl sulfate, pyocyanin, and 1-hydroxyphenazine, were purchased from Cayman Chemical Company. Benzo(A)phenazine-7,12-dioxide, phenazine, neutral red, phenazine ethosulfate, phenazine methosulfate, phenazine-1-carboxamide, 3-(N-morpholino)propane sulfonic acid (MOPS), N,N-dimethylformamide (anhydrous, 99.8%), ethanol, and tetrabutylammonium hexafluorophosphate ($TBAPF_6$) were acquired from Sigma-Aldrich. D-glucose (glucose) and magnesium chloride ($MgCl_2$) were obtained from Fisher Scientific Inc.

Phenazine mediator preparation

This study evaluated and characterized nine phenazine mediators, including (1) neutral red (NR), (2) pyocyanin (PYO), (3) 1-methoxy-5-methylphenazinium methyl sulfate (MPMS), (4) benzo(A)phenazine-7,12-dioxide (BAPD), (5) phenazine methosulfate (PMS), (6) phenazine ethosulfate (PES), (7) phenazine (PHZ), (8) 1-hydroxyphenazine (OHPHZ), and (9) phenazine-1-carboxamide (PCX), using a concentration of 100 μM for each mediator. The mediators were characterized using cyclic voltammetry in both aqueous buffer and aprotic media. A 2 mM stock solution for each mediator was prepared in (1) 20 mM MOPS buffer (pH 7) containing 10 mM $MgCl_2$ and 100 mM glucose, and (2) N,N-dimethylformamide (DMF) with 0.1 M $TBAPF_6$ as the aqueous and aprotic electrolyte solutions, respectively. The 2 mM phenazine mediator stock solutions were initially stabilized with 20% ethanol, giving a final concentration below 0.1% in the electrolyte solutions. Namely, the 2 mM stock solution for each phenazine was diluted to 500 μM stock solution in either the aqueous MOPS buffer or aprotic media solution. Using the 500 μM stock solutions, 100 μM solutions of each phenazine mediator were prepared in each electrolyte solution for evaluation of its electrochemical behavior in both aqueous and aprotic media.

Electrochemical setup

Electrochemical measurements were performed using a three-electrode cell setup at room temperature ($20 \pm 1°C$). The electrochemical behavior and redox response for the nine different phenazine mediators were examined using cyclic voltammetry (CV) experiments (using either a Squidstat Prime potentiostat (Admiral Instruments) or a CH660 potentiostat (CH Instruments)). In this study, the working electrodes utilized were AvCarb carbon paper electrodes (AvCarb MGL 190, Fuel Cell Store) with an area of 1 cm^2 and the counter electrode was a Pt mesh electrode. For phenazine mediator characterization in aqueous media, a saturated calomel electrode (SCE) was used as the reference electrode while for phenazine mediator characterization in aprotic media, a silver/silver nitrate ($Ag/AgNO_3$ labeled as Ag/Ag^+) non-aqueous reference electrode was used as the reference electrode. Thus, for studies in aqueous and aprotic media, the potentials discussed in this paper refer to the SCE and Ag/Ag^+ non-aqueous reference electrodes, respectively. The electrolyte solutions were 20 mM MOPS buffer (pH 7) + 10 mM $MgCl_2$ + 100 mM glucose, and 0.1 M $TBAPF_6$ in DMF for electrochemical experiments. For studies in the aqueous buffer, CV tests were performed at varying scan rates of 5, 10, 25, 50, 75, 100, and 250 mV s^{-1}. For tests in the aprotic media, CV measurements were obtained at a scan rate of 5 mV s^{-1}. Before performing CV tests in aprotic media, the Ag/Ag^+ reference electrode was calibrated using ferrocene standard solution (2 mM ferrocene in 0.1 M $TBAPF_6$ in DMF). Dependent on the type of phenazine mediator, specific and different potential windows were used for CV data in aqueous and aprotic media, which can be found in Figures S1 and S3 in the supplemental information. All CV tests in aqueous and aprotic media were performed in triplicate and the average values of the resulting CV current responses were used. Details on *E. coli* cell growth, bacteria immobilization on working electrode surfaces, electrochemical setup for amperometric constant-potential *i-t* measurements used to calculate the mediated current densities utilized for modeling and discussed in this work are described in our previous study (Simoska et al., 2021), in which each experiment was performed five times.

Density functional theory

Density functional theory (DFT) computations were first carried out through a geometry optimization in the gas phase with the M06-2X/6-31 + g(d,p) level of theory (Hehre et al., 1972, Zhao and Truhlar 2008a, b) and a tight convergence criteria (int = ultrafine) using the Gaussian16 (revision C.01) Software Package (Frisch et al., 2016). Minimized energy structures were confirmed with a frequency calculation (zero imaginary frequencies). The gas-phase optimized geometries were used for all calculations in this work. Following this optimization step, a single-point energy calculation was performed using the M06-2X/jun-cc-pvtz level of

theory (Hariharan and Pople 1973; Weigend and Ahlrichs 2005) for more accurate free energies of the ground state for each phenazine molecule. A final single-point calculation was performed at the same level of theory (M06-2x/jun-cc-pvtz) in water utilizing a continuum solvation model based on the quantum mechanical electron density of the molecule (solvent model "density") SMD model (Marenich et al., 2009a, b) with each of the phenazine mediators. Gaussian defaults were used in all computations unless previously specified.

Multivariate linear regression modeling

The understanding of disparate rates of current densities with differing phenazine mediators was evaluated via the use of multivariate linear regression (MLR) modeling. Molecular parameters were isolated from the oxidized low-energy conformers in condensed phase for each of the phenazines in the training set. These were generated using both DFT with Gaussian16 (Frisch et al., 2016) and molecular mechanics (MM) through the QikProp (Schrödinger Release, 2021-2: QikProp, 2021) package in MacroModel, focusing on parameters that were hypothesized to describe mediator reduction potential and interaction with the cellular membrane (e.g., reduction potential, polarity, lipophilicity, size, volume). MLR model development and predictions were performed using MATLAB R2018b software (MATLAB R2017b, 2017) with the generated molecular descriptors as described previously (Guo et al., 2017; Santiago et al., 2018; Sigman et al., 2016) using normalized parameters by subtracting the mean of each value and dividing by the standard deviation.